*Proceeding Paper*

# Analysis of Baseband Algorithms for LEO PNT [†]

**Fran Fabra [1,*] , José A. López-Salcedo [1,2] and Gonzalo Seco-Granados [1,2]**

1    Institut d'Estudis Espacial de Catalunya (IEEC), 08034 Barcelona, Spain; jose.salcedo@uab.cat (J.A.L.-S.); gonzalo.seco@uab.cat (G.S.-G.)
2    Department of Telecommunication and Systems Engineering, Universitat Autònoma de Barcelona (UAB), 08193 Bellaterra, Spain
*    Correspondence: fabra@ieec.cat
†    Presented at the European Navigation Conference 2023, Noordwijk, The Netherlands, 31 May–2 June 2023.

**Abstract:** This paper provides an analysis of the impact of transmitter dynamics on baseband algorithms for position, navigation and timing applications using a low Earth orbit constellation. In particular, the acquisition and tracking of signals with high dynamics have larger Doppler and Doppler drift values that might impair the use of standard methods. Our analysis combines a theoretical assessment of acquisition and tracking thresholds with a performance evaluation by means of a simulation. Three frequency bands are tested (UHF, S and Ka) and an open-source software receiver has been adapted for such a purpose. The results obtained show the potential feasibility of LEO-PNT at baseband level under minimal considerations.

**Keywords:** LEO-PNT; GNSS; acquisition; tracking

## 1. Introduction

The high demand on Position Navigation and Timing (PNT) solutions, plus the advent of several Low Earth Orbit (LEO) constellations, has brought attention to the use of these signals for PNT applications [1–3]. Compared with traditional Global Navigation Satellite Systems (GNSS), LEO signals benefit from higher power transmission, a greater number of satellites, faster multipath conditions, and a lower cost of deployment, which enables the more frequent replacement of constellation generation.

From a baseband point of view, LEO-based PNT is characterized by high dynamics signals due to the larger Doppler shift induced by the relatively high velocity of the transmitter [4]. This means an increase in computation time during acquisition due to the larger search space. Moreover, in severe Doppler conditions, code-frequency offset (also referred to as code Doppler) can also be significant and needs to be compensated [5]. Considering that the visibility time window of a LEO satellite is also smaller, external aiding might be a mandatory condition for acquiring signals in certain frequency bands. Regarding tracking, the increase of Doppler-rate under high dynamics might cause phase, frequency and code deviations that cannot be followed using traditional tracking configurations in standard GNSS receivers (there is a larger probability of tracking loss due to dynamic stress error).

The analysis presented in this paper is split in two parts. First, a theoretical assessment is carried out to evaluate the acquisition and tracking thresholds for a set of signals considered (ranging from UHF to Ka bands) under the corresponding Doppler and Doppler rates from a LEO constellation. In the second part, the previous results are compared against a simulation analysis based on Monte Carlo realizations of the different signals under the selected scenarios.

## 2. Theoretical Assessment

In order to evaluate the potential frequency diversity of LEO-PNT systems, three bands have been preliminary selected in the present study: UHF, S and Ka. For each case,

spread-spectrum GNSS-like signals have been considered, and no navigation message has been included.

In a standard LEO use case scenario, the dynamics will be mainly driven by the satellite motion. Table 1 shows the dynamics considered in the following analysis derived from the assumed LEO constellation (maximum values and comparison with GPS [6] as a reference).

**Table 1.** User–satellite range dynamics for LEO scenario and GPS.

| Range Derivative | LEO | GPS |
|:---:|:---:|:---:|
| $\dot{\rho}$ | 7000 m/s | 800 m/s |
| $\ddot{\rho}$ | 90 m/s$^2$ | 0.14 m/s$^2$ |
| $\dddot{\rho}$ | 1 m/s$^3$ | 0.000122 m/s$^3$ |

*2.1. Acquisition Thresholds*

We will evaluate here the impact of LEO dynamics on signal acquisition and compare the results obtained against those from GPS L1, which will serve as a reference. The first parameter that we can check is the number of Doppler bins needed to cover the whole dynamic range. For a given code length, such a parameter gives the number of cells that need to be scanned during a cold start, thus providing some information about its feasibility as a real-time application for a given receiver. Table 2 provides the number of Doppler bins (computed as one half of the inverse of the coherent integration time) for two values of coherent integration time ($T_{co}$): the code period of the corresponding component for each signal and 10 ms. The next step is to check the impact of the Doppler change during the coherent integration. For this purpose, Table 2 also provides the amount of Doppler drift as a percentage of the Doppler bin. The results obtained for 10 ms of coherent integration reveal the problems that would be faced when trying to acquire signals at high frequency bands, where the coherent accumulation would not efficiently increase the signal-to-noise ratio without external assistance to correct the Doppler drift.

**Table 2.** Acquisition parameters for the different signals under analysis.

| Frequency Band | GPS L1 | UHF | S | Ka |
|:---|:---:|:---:|:---:|:---:|
| Doppler bins ($T_{co} = T_{code}$) | 17 | 30 | 117 | 115 |
| Doppler drift over bin [%] | 0.0001 | 0.015 | 0.037 | 0.003 |
| Doppler bins ($T_{co} = 10$ ms) | 169 | 382 [1] | 2328 | 28627 |
| Doppler drift over bin [%] | 0.01 | 2.55 [1] | 14.96 | 184.03 |

[1] Actual $T_{co}$ for UHF is 10.4 ms to be an integer multiple of the corresponding $T_{code}$.

Finally, we follow the procedure summarized in [7] to compute the probability of detection during the acquisition process as follows:

$$P_d = 1 - F_{(\chi^2(2K,\beta))}\left(T_h^{\text{acq}}\right), \tag{1}$$

where $F_{(\chi^2(2K,\beta))}$ is the cumulative distribution function of a non-central $\chi^2$ distribution with $2K$ degrees of freedom (with $K$ being the number of incoherent accumulations) and a non-centrality parameter $\beta$, which is approximated, because the delay and Doppler uncertainties are not accounted for:

$$\beta = \frac{C}{N_0} K T_{co}. \tag{2}$$

The threshold value $T_h^{\text{acq}}$ is computed from a desired probability of false alarm $P_{\text{fa}}$ as follows:

$$T_h^{\text{acq}} = F_{(\chi^2(2K))}^{-1}(1 - P_{\text{fa}}). \tag{3}$$

By combining the previous expressions and fixing desired values for $P_d$ and $P_{\text{fa}}$, we can scan over $C/N_0$ to obtain the acquisition threshold. Table 3 shows the results obtained when considering the whole search space for each type of signal according to the code length and Doppler range.

**Table 3.** Acquisition threshold to achieve $P_d = 0.95$ with a $P_{\text{fa}} = 0.001$ [dB-Hz].

| Frequency Band | GPS L1 | UHF | S | Ka |
|---|---|---|---|---|
| $T_{co} = T_{code}$ | 47.6 | 48.9 | 51.2 | 62.1 |
| $T_{co} = 10$ ms | 37.9 | 38.2 [1] | 38.7 | 38.9 |

[1] Actual $T_{co}$ for UHF is 10.4 ms to be an integer multiple of the corresponding $T_{code}$.

### 2.2. Tracking Thresholds

We will evaluate here the tracking performance of the different signals under analysis. A set of representative configurations of the delay, frequency and phase lock loops will be analysed by following the procedures from [8].

In general, the rule-of-thumb for setting the tracking threshold is to apply the following:

$$\sigma_{\text{track}} + e_d/3 \le T_h^{\text{track}}, \tag{4}$$

where the particular values of tracking jitter $\sigma_{\text{track}}$, dynamic stress error $e_d$ and threshold limit $T_h^{\text{track}}$ for each type of loop are given in Table 4. Details on the jitter computation for delay (DLL), frequency (FLL) and phase lock loops (PLL) will be described later. The impact of these dynamics is mainly determined by the derivatives of the line-of-sight range $\rho$ and the natural frequency of the loop filter of $n$-order $\omega_0$, which is proportional to the loop noise bandwidth $B_n$. We take $B_n = 0.53\omega_0$ for a second-order filter and $B_n = 0.7845\omega_0$ for a third-order filter. Finally, the threshold limits for DLL depend on the early-to-late distance $D$ of the discriminator. In the case of FLL, this value is a function of the integration time $T$, while for PLL it is fixed to $30°$ because we consider a data-less four-quadrant arctangent discriminator.

**Table 4.** Terms for tracking threshold computation depending on type of loop.

| Term | DLL | FLL | PLL |
|---|---|---|---|
| $\sigma_{\text{track}}$ | $\sigma_{\text{DLL}}$ | $\sigma_{\text{FLL}}$ | $\sigma_{\text{PLL}}$ |
| $e_d$ | $\rho_e = \dfrac{d^n\rho/dt^n}{\omega_0^n}$ | $f_e = \dfrac{d^{n+1}\rho/dt^{n+1}}{\lambda\omega_0^n}$ | $\theta_e = \dfrac{360}{\lambda}\dfrac{d^n\rho/dt^n}{\omega_0^n}$ |
| $T_h^{\text{track}}$ | $D/6$ | $1/12T$ | $30°$ |

The general expression for thermal noise code tracking jitter $\sigma_{\text{DLL}}$ is given by the following:

$$\sigma_{\text{DLL}} = c\sqrt{\frac{B_n \int_{-B_{fe}/2}^{B_{fe}/2} S_s(f)\sin^2(\pi f D T_c)df}{(2\pi)^2 C/N_0(\int_{-B_{fe}/2}^{B_{fe}/2} f S_s(f)\sin(\pi f D T_c)df)^2}\left(1 + \frac{\int_{-B_{fe}/2}^{B_{fe}/2} S_s(f)\cos^2(\pi f D T_c)df}{TC/N_0(\int_{-B_{fe}/2}^{B_{fe}/2} f S_s(f)\cos(\pi f D T_c)df)^2}\right)}, \tag{5}$$

where $c$ is the speed of light, $B_{fe}$ is the front-end bandwidth, $S_s(f)$ is the power spectral density of the signal, normalized to unit area over infinite bandwidth, $T$ is the pre-detection integration time and $T_c = 1/R_c$ is the chip period (the inverse of the chipping rate).

Then, the tracking thresholds can be computed by determining the $C/N_0$ value required to obtain an equality in the aforementioned rule-of-thumb for the stress error level

given by the LEO dynamics. Table 5 provides the results for DLL, where we can see the impact of dynamics in the improvement obtained when using third-order loop architectures in the LEO cases. The integration time is set to the corresponding $T_{code}$ (the wide-band component for the LEO cases).

**Table 5.** Tracking threshold for DLL [dB-Hz].

| Frequency Band | GPS L1 | UHF | S | Ka |
|---|---|---|---|---|
| $B_n = 2$ Hz, 2nd order | 22.7 | 20.7 | 25.9 | - |
| $B_n = 2$ Hz, 3rd order | 22.7 | 18.6 | 20.0 | 25.0 |
| $B_n = 18$ Hz, 2nd order | 27.9 | 24.5 | 25.6 | 30.1 |
| $B_n = 18$ Hz, 3rd order | 27.9 | 24.5 | 25.6 | 29.7 |

The frequency tracking jitter due to thermal noise is given by the following:

$$\sigma_{\text{FLL}} = \frac{1}{2\pi T} \sqrt{\frac{4FB_n}{C/N_0} \left(1 + \frac{1}{TC/N_0}\right)}, \tag{6}$$

where the term $F$ is set to 1 and changes to 2 when the result is near the threshold. The results obtained for the different signals and configurations are shown in Table 6. Again, we can see the improvement obtained when increasing the order of the filter in LEO cases, especially for low values of $B_n$.

**Table 6.** Tracking threshold for FLL [dB-Hz].

| Frequency Band | GPS L1 | UHF | S | Ka |
|---|---|---|---|---|
| $B_n = 2$ Hz, 1st order | 24.4 | 23.5 | 41.5 | - |
| $B_n = 2$ Hz, 2nd order | 24.4 | 21.5 | 22.7 | 27.2 |
| $B_n = 18$ Hz, 1st order | 30.2 | 28.6 | 29.7 | 33.1 |
| $B_n = 18$ Hz, 2nd order | 30.2 | 28.3 | 29.0 | 32.4 |

Finally, the phase tracking jitter due to thermal noise is given by the following:

$$\sigma_{\text{PLL}} = \frac{360}{2\pi} \sqrt{\frac{B_n}{C/N_0} \left(1 + \frac{1}{2TC/N_0}\right)}. \tag{7}$$

It is important to remark that we are neglecting two other relevant components of the total phase jitter: the Allan deviation oscillator noise and the vibration-induced noise. The reason for this is that we prefer to focus on the impact of dynamics in the present study. However, as described in [9], these terms are directly proportional to the carrier frequency, so their impact will be especially relevant for high frequency bands and thus should be carefully analyzed in the implementation of LEO PNT test platforms.

Table 7 provides the results obtained for the different signals and configurations. We can see how the dynamics in LEO disable the possibility of reaching acceptable values in most of the scenarios and that second-order loops are not a valid option.

**Table 7.** Tracking threshold for PLL [dB-Hz].

| Frequency Band | GPS L1 | UHF | S | Ka |
|:---:|:---:|:---:|:---:|:---:|
| $B_n = 2$ Hz, 2nd order | 24.0 | - | - | - |
| $B_n = 2$ Hz, 3rd order | 21.4 | 16.8 | - | - |
| $B_n = 18$ Hz, 2nd order | 27.2 | 24.2 | - | - |
| $B_n = 18$ Hz, 3rd order | 27.1 | 20.8 | 21.8 | 26.2 |

## 3. Simulation Analysis

Each of the LEO signals described have been simulated assuming a constellation at an altitude of 600 km. With the aim of covering most of the Doppler and Doppler drift ranges at each frequency band, seven satellites have been simultaneously generated at different elevations to build 4 s of raw samples. This datasets are then injected into a modified version of FGI-GSRx [10,11], an open-source GNSS receiver. In addition to the adaptation of the particular characteristics of our LEO signals (modulation and code properties), the modification includes code Doppler compensation in terms of acquisition and a new tracking loop engine that implements a second-order DLL with a third-order PLL aided by a second-order FLL.

### 3.1. Results for Acquisition

The acquisition analysis consists in performing 1000 realizations of data, with added white Gaussian noise (adapted to a given $C/N_0$ value), to obtain the corresponding metrics employed to determine the signal presence during the acquisition process. The value of the fifth percentile (5%), which would correspond to a probability of detection of 0.95, is compared to the acquisition threshold for a probability of false alarm of 0.001 (the computation of this term takes into account the total number of code-Doppler cells required during a full acquisition process). Figure 1 provides the results obtained for the same LEO cases shown previously in Table 3. We can see that there is a generally good agreement with the theoretical assessment, including the case at the Ka band with longer integration. Therefore, the lack of Doppler drift aiding does not have a strong impact in these scenarios.
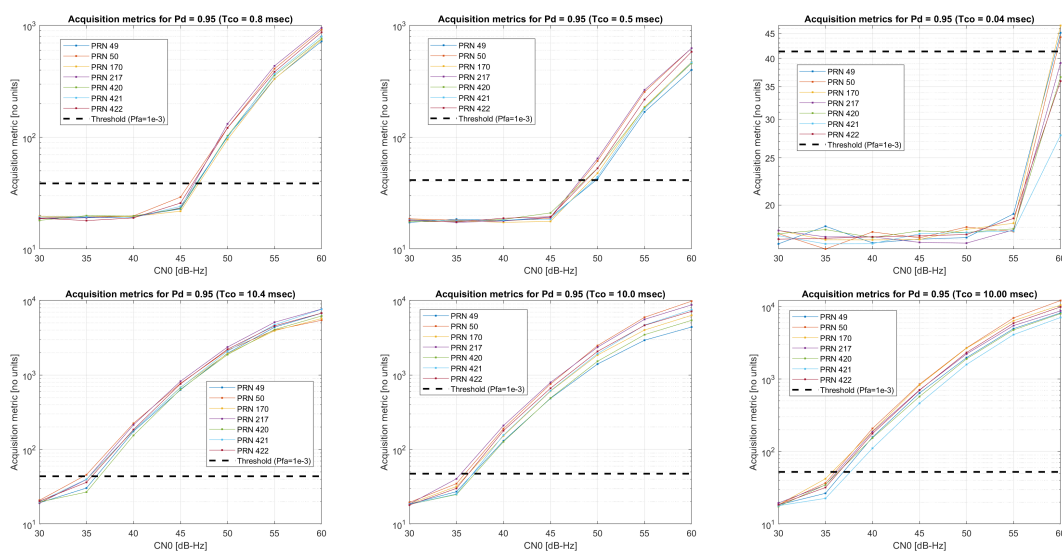


**Figure 1.** Acquisition results from simulation analysis. A dashed line indicates the corresponding threshold limit for a probability of false alarm of 0.001. Columns from left to right: results from UHF, S and Ka bands. **Upper row**: $T_{co} = T_{code}$. **Bottom row**: $T_{co} = 10$ ms (10.4 ms for UHF).

### 3.2. Results for Tracking

For tracking analysis, the procedure consists in performing the acquisition of noise-free data and starting tracking with a wide loop bandwidth (40 Hz) in order to safely reach a steady state in a short time interval and to then include additive white Gaussian noise and to set a given loop bandwidth. Then, the resultant code, phase and Doppler evolution are compared against the corresponding models to estimate the error values as the standard deviation of such differences over the given interval (from seconds 3 to 4) and averaged after 10 different iterations. Figures 2–4 provide the code, phase and Doppler output error results for the loop bandwidth values employed during the theoretical assessment. In order to limit the number of different combinations, the same loop bandwidth is applied to the three different loops of the implemented architecture. The integration time is set to the code period of the corresponding wide band component. Regarding the obtained results, the code-tracking thresholds that can be derived from the graphs are well aligned with the theoretical values for third-order loops given in Table 5 (recall that our second-order DLL is aided by a third-order PLL/FLL loop). On the other hand, the frequency results seem to benefit from the combination with the phase discriminator in the loop architecture. However, such a combination also has an impact on the phase, which provides more robust results for $B_n = 2$ Hz (tracking is achieved), while worsening the expectation when using a larger loop bandwidth value (the thresholds seem to be bounded by the performance of the FLL). It is also relevant to point out the results in frequency and phase from PRN 421, which are probably due to the fact that this was the satellite with the highest Doppler drift.
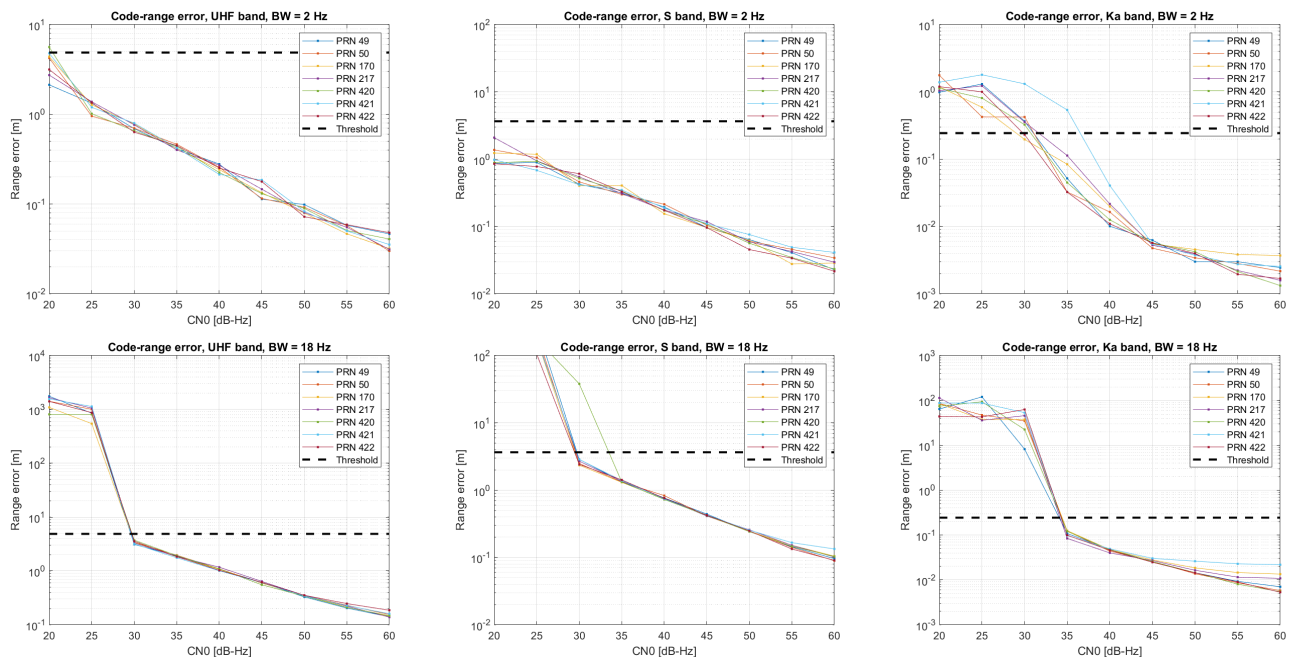


**Figure 2.** Tracking code results from simulation analysis. A dashed line indicates the corresponding threshold limit. Columns from left to right: results from UHF, S and Ka bands. **Upper row**: $B_n = 2$ Hz. **Bottom row**: $B_n = 10$ Hz.
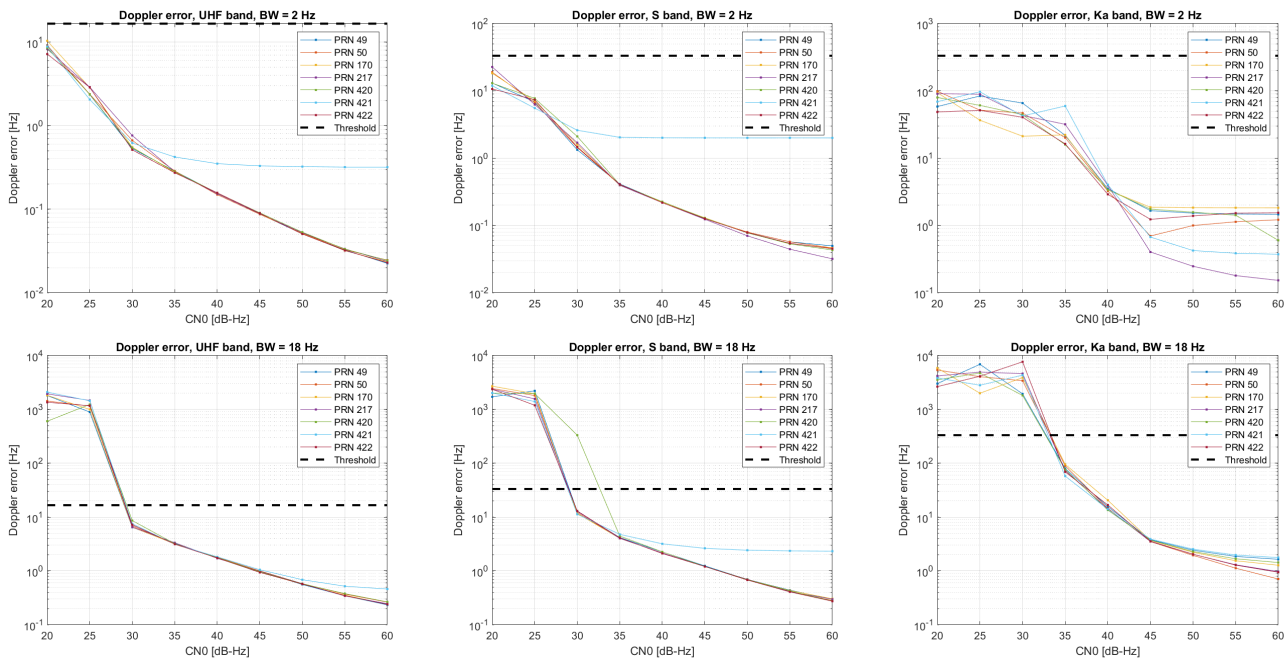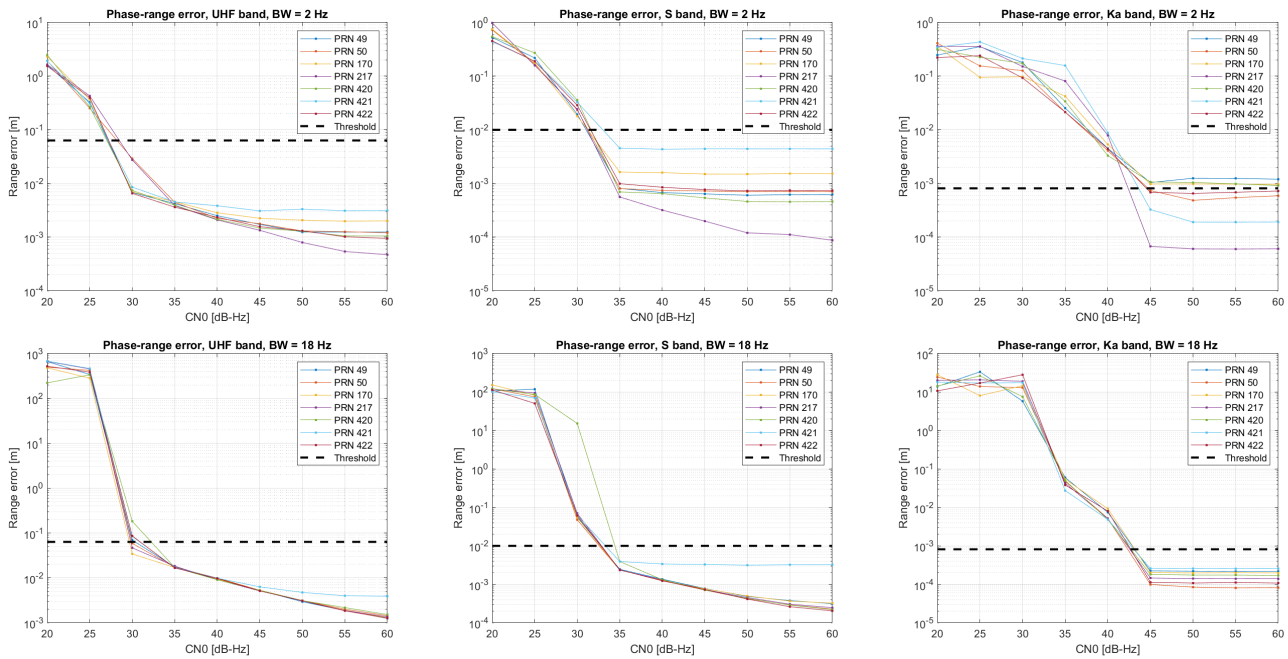
**Figure 3.** Tracking frequency results from simulation analysis. A dashed line indicates the corresponding threshold limit. Columns from left to right: results from UHF, S and Ka bands. **Upper row**: $B_n = 2$ Hz. **Bottom row**: $B_n = 10$ Hz.



**Figure 4.** Tracking phase results from simulation analysis. A dashed line indicates the corresponding threshold limit. Columns from left to right: results from UHF, S and Ka bands. **Upper row**: $B_n = 2$ Hz. **Bottom row**: $B_n = 10$ Hz.

## 4. Discussion

The analysis presented in this paper shows the potential feasibility of LEO-PNT at baseband level. Compared with the standard GNSS, LEO-PNT will typically have higher demanding acquisition thresholds which can be compensated for with higher received power levels. The large Doppler ranges imply a higher number of Doppler cells, thus significantly increasing the total number of search cells. Although this might not be a limitation in terms of acquisition thresholds, it can have a strong impact on real-time

implementations. However, this effect could be compensated for by means of Doppler aiding. The most relevant aspect in our software-based GNSS receiver is the necessity of including code Doppler correction to enable longer integration times.

Regarding tracking, the theoretical assessment shows that only high-order loops can be used to properly track the LEO dynamics (even considering a static receiver). Despite this, the tracking loop architecture implemented has shown the capability of successfully tracking the selected signals in the different bands under analysis. However, it is worth mentioning that neither clock- or vibration-induced errors have been included, which have an important impact on high frequency bands.

## Abbreviations

The following abbreviations are used in this manuscript:

| | |
|---|---|
| LEO | Low Earth Orbit |
| PNT | Positioning, Navigation and Timing |
| UHF | Ultra-High Frequency |
| GNSS | Global Navigation Satellite System |
| GPS | Global Positioning System |
| DLL | Delay Lock Loop |
| FLL | Frequency Lock Loop |
| PLL | Phase Lock Loop |

## References

1. Benzerrouk, H.; Nguyen, Q.; Fang, X.; Amrhar, A.; Rasaee, H.; Landry, R. LEO satellites Based Doppler Positioning Using Distributed nonlinear Estimation. *IFAC-PapersOnLine* **2019**, *52*, 496–501. [CrossRef]
2. Cheng, L.; Dai, Y.; Guo, W.; Zheng, J. Structure and Performance Analysis of Signal Acquisition and Doppler Tracking in LEO Augmented GNSS Receiver. *Sensors* **2021**, *21*, 525. [CrossRef] [PubMed]
3. Kassas, Z.; Morales, J.; Khalife, J. New-age satellite-based navigation–STAN: Simultaneous tracking and navigation with LEO satellite signals. *Inside GNSS Mag.* **2019**, *14*, 56–65.
4. Ali, I.; Al-Dhahir, N.; Hershey, J.E. Doppler Characterization for LEO Satellites. *IEEE Trans. Commun.* **1998**, *46*, 309–313. [CrossRef]
5. Cheng, U.; Hurd, W.J.; Statman, J.I. Spread-Spectrum Code Acquisition in the Presence of Doppler Shift and Data Modulation. *IEEE Trans. Commun.* **1990**, *38*, 241–250. [CrossRef]
6. Misra, P.; Enge, P. *Global Positioning System, Signals, Measurements, and Performance*, 2nd ed.; Ganga-Jamuna Press: Lincoln, MA, USA, 2006.
7. Foucras, M.; Julien, O.; Macabiau, C.; Ekambi, B.; Bacard, F. Assessing the Performance of GNSS Signal Acquisition: New Signals and GPS L1 C/A Code. Inside GNSS, Inside GNSS Media LLC. 2014; pp. 68–79. Available online: https://insidegnss.com/wp-content/uploads/2018/01/IGM_julaug14-WP.pdf (accessed on 10 January 2023).
8. Kaplan, E.D.; Hegarty, C.J. *Understanding GPS: Principles and Applications*, 2nd ed.; Artech House: Boston, MA, USA, 2006.

9. Irsigler, M.; Eissfeller, B. PLL tracking performance in the presence of oscillator phase noise. *GPS Solut.* **2002**, *5*, 45–57. [CrossRef]
10. FGI-GSRx Software Receiver. Available online: https://github.com/nlsfi/FGI-GSRx (accessed on 15 May 2023).
11. Borre, K.; Fernández-Hernández, I.; Lopez-Salcedo, J.A.; Bhuiyan, M.Z.H. *GNSS Software Receivers*; Cambridge University Press: Cambridge, UK, 2022, *in press*.